Arabian Journal of Chemistry (2020) 13, 5474–5486

King Saud University

Arabian Journal of Chemistry

www.ksu.edu.sa
www.sciencedirect.com

ORIGINAL ARTICLE

Removal of phenol from aqueous solution by adsorption onto hematite (α-Fe_2O_3): Mechanism exploration from both experimental and theoretical studies

Younes Dehmani [a], Awad A. Alrashdi [b], Hassane Lgaz [c,*], Taibi Lamhasni [d], Sadik Abouarnadasse [a], Ill-Min Chung [c,*]

[a] *Laboratory of Chemistry and Biology Applied to the Environment, Moulay Ismail University, Faculty of Sciences of Meknes, Meknes, Morocco*
[b] *Chemistry Department, Umm Al-Qura University, Al-Qunfudah University College, Saudi Arabia*
[c] *Department of Crop Science, College of Sanghur Life Science, Konkuk University, Seoul 05029, South Korea*
[d] *Institut National des Sciences de l'Archéologie et du Patrimoine (INSAP), BP 6828, Madinat al Irfane, Avenue Allal El Fassi, Angle rues 5 et 7, Rabat-Instituts, Morocco*

Received 11 February 2020; accepted 28 March 2020
Available online 2 April 2020

KEYWORDS

Adsorption;
Organic pollutants;
Hematite;
DFT;
Molecular dynamics

Abstract Iron oxides in general and especially hematite, α-Fe_2O_3 have been proved promising materials for efficient removal of various organic pollutants. Herein, we report a successful preparation of hematite (α-Fe_2O_3) by a facile precipitation method and its potential application in the removal of phenol from wastewater. The prepared material was subjected to extensive characterization using a variety of techniques such as scanning electron microscope coupled with energy-dispersive X-ray spectroscopy (SEM/EDX), X-ray diffraction (XRD), and the Brunauer Emmett Teller (BET) method. The operating conditions were optimized to improve the adsorption process efficiently. The adsorption analysis showed an adsorption capacity of 16.17 mg g^{-1} towards phenol at 30 °C. The reaction kinetics and potential rate-limiting steps were studied by Lagergren's pseudo-first-order and pseudo-second-order models, and it was found that the pseudo-second-order accurately described the adsorption kinetics. Freundlich and Langmuir adsorption isotherms models were applied, and the quality of the fittings clearly shows that the Langmuir model well describes the phenol adsorption on the hematite. The interaction mechanism between phenol and α-Fe_2O_3(0 0 1) surface was further addressed by Density Functional Theory (DFT) calculations

* Corresponding authors.
E-mail addresses: hlgaz@konkuk.ac.kr (H. Lgaz), imcim@konkuk.ac.kr (I.-M. Chung).
Peer review under responsibility of King Saud University.

ELSEVIER Production and hosting by Elsevier

https://doi.org/10.1016/j.arabjc.2020.03.026

and molecular dynamics (MD) simulations. Experimental and theoretical results indicate that there is strong evidence for the decisive effect of π–π interactions and H-bonds on the adsorption capacity.

1. Introduction

Environmental pollution, especially organic pollutants, represents an essential threat to human health and natural ecosystems globally (Ali, 2018; Chatterjee and Dasgupta, 2005; Elsagh et al., 2017). Indeed, volatile organic compounds (VOC), including phenols, aldehydes, aromatic hydrocarbons, etc. are associated with a broad range of industrial processes and applications as refrigerants, solvents, reactive agents, among others. Still, their discharge into the atmosphere without an appropriate control can threaten the environment and leads to serious health problems to humans, animals, and aquatic systems (Ahmed et al., 2016; Arumugam et al., 2018; Banerjee and Chattopadhyaya, 2017; Pathania et al., 2017; Sartape et al., 2017; Somasekhara Reddy et al., 2017). It is generally known that the phenol, which is a semi-volatile organic compound (SVOC) and widely existing in medical and industrial wastewaters, and oil-refining wastes, is a persistent organic pollutant that is hard to degrade in nature (Vosoughi et al., 2017). Contact of phenol with the surrounding skin and respiratory tract can lead to human poisoning. In this case, a higher concentration of phenol can cause protein precipitation that leads to direct damage to cells, and even at low concentrations can still induce protein denaturation (Shen et al., 2019). Therefore, the removal of phenol in a cost-effective and environment-friendly manner is an effective way to protect the environment and secure human health (Gautam et al., 2018).

To date, a variety of methods has been proposed to remove phenols from wastewaters. For instance, ion exchange, chemical precipitation, chemical and electrochemical oxidation, photochemical processes ozonation, and Fenton processes are among the most commonly used methods (Villegas et al., 2016). These methods, however, accompanied by a drawback that they require relatively high expenses on energy and catalysts. With respect to this, adsorption can be regarded as a promising method to remove organic pollutants from water due to its simple implementation, its high efficiency, its cost-effectiveness and versatility under different operating conditions (Hwang et al., 2017).

Oxides have repeatedly proved their high efficiency in the removal of organic pollutants from wastewater (Essandoh and Garcia, 2018). Among them are iron oxides, which are one of the most abundant mineral groups on Earth and have proven to be useful in many different applications at the research and industrial levels. There is a widespread belief that these environment-friendly materials have a high potential in a wide range of applications, especially in magnetization, biomedical science, catalysis, and environmental applications. Interestingly, they have shown excellent potential as adsorbents for the removal of environmental pollutants because of their faster adsorption rate, higher adsorption affinity and capacity and large surface areas in comparison to many other adsorbents (Essandoh and Garcia, 2018; Y.-L. Ge et al., 2019; Milagres et al., 2020). The preparation method, precursors, and precipitation agents of iron oxides have a significant effect on their structural and textural properties and thus on their activity.

An extensive amount of work on the adsorption of organic compounds onto synthetic iron oxides has already been published (Das et al., 2005). For instance, Parfitt et al. (Parfitt et al., 1977) prepared the goethite (α-FeOOH) and studied its potential for adsorption of oxalic acid. Hwang et al. (Hwang et al., 2007) synthesized the hematite (α-Fe_2O_3), which removes o-phthalic acid efficiently under a wide range of environmental conditions. Das et al. have used natural hematite successfully for the removal of benzoate and salicylate (Das et al., 2005).

Although there is now extensive research ongoing worldwide to investigate the potential of iron oxides to function as adsorbent materials, experimental information is not always enough, and there remaining much to be learned to better understand mechanisms and interactions of organic pollutants with iron oxides. In this context, computer simulation methods are getting increasing importance in predicting stable adsorption complexes and providing detailed insight into interaction mechanisms (Harris, 2019). Recently, Density Functional Theory (DFT) has been extensively used as a tool to clarify some questions and to provide deeper insights in various chemical and physical fields including adsorption and catalysis (Kuznetsov et al., 2015; Li et al., 2018; Novikov et al., 2016, 2013). In the last few years, DFT calculations have been used to study the adsorption structures of Sb(V), Sb(III), Se(IV), Cr (VI) as well as H_2S and surfactants on hematite surfaces (Dzade et al., 2014). On the other hand, molecular dynamics simulation is a beneficial method to get insightful knowledge about interaction mechanisms between adsorbate and adsorbent in a simulated environment. Many researchers used this method to provide some explanation about the adsorption mechanism and offer guidance to design effective adsorbents (Guediri et al., 2020; Hosseini et al., 2019; Kuntail et al., 2019; Zhang et al., 2019).

In this paper, we report the facile preparation of hematite (α-Fe_2O_3) by the precipitation method and its potential application in the removal of phenol from wastewater. The structural and morphological characteristics of the prepared hematite were determined based on adsorption/desorption of nitrogen gas, SEM/EDX, and X-ray diffraction methods. At the same time, its potential for phenol removal from wastewater was evaluated under different operating parameters such as pH, initial concentration, and temperature. Furthermore, the adsorption of phenol on the α-Fe_2O_3 surface was investigated and discussed by DFT calculations, and MD simulations and a possible binding mechanism of phenol on the α-Fe_2O_3 surface was inferred.

2. Materials and methods

2.1. Preparation of adsorbent

The hematite material was obtained as follows: An amount of iron nitrate dihydrate ($Fe(NO_3)_3$, $9H_2O$) was dissolved in distilled water, and this solution was vigorously stirred for 2 h at room temperature to form a homogeneous solution. To this mixture, a molar solution of aqueous ammonia (NH_4OH) was added dropwise (7 ml/min) 20 ml, and the formation of a colloidal solution was achieved. The resulting mixture was heated under constant stirring at 40 °C for 1 h and then filtered under vacuum. The resulting solid was washed thoroughly several times with distilled water and dried overnight in an oven at 100 °C. The resultant crude solids were heat-treated in the air at 500 °C for 3 h.

2.2. Characterization of adsorbent

The crystalline structure was determined using an X-ray Brucker diffractometer (XRD, Brucker-AXS D8), and 1.541838 Å Cu-Kα radiation was used to collect XRD patterns, operating at 40 kV and a current of 40 mA. BET (Brunner, Emmett, and Teller) N_2 adsorption–desorption method was used to obtain the textural parameters like pore diameter, specific surface area, as well as their distribution and volumes. BET experiments were conducted at −196.15 °C on a Micromeritics ASAP 2010 analyzer (USA). Prior to N_2 adsorption, samples were degassed under vacuum during a determined period at a given temperature. Scanning electron microscope (SEM) (FEI Quanta 200 equipped with an EDX device and operating at 18 keV) was used to determine the elemental distribution and surface morphology of the prepared material.

2.3. Phenol adsorption

Adsorption experiments were studied at different constant temperatures (30, 40, 50, and 60 °C). Prior to the commencement of the experiment, the initial pH of the simulated phenol solution was adjusted when necessary with NaOH or HCl. For batch experiments, hematite iron oxide in an amount of 0.1 g was added to a 20 ml of phenol at different initial concentrations with the stirring speed set at 600 rpm. At the predetermined equilibration time, the residual concentration (C_e) in the solution of the phenol was determined using UV/Visible spectrometer (Shimadzu, UV-1240) by measuring the maximum absorption at 270 nm. From residual concentration (C_e in mg/L) and initial concentration (C_o in mg/L), and the amount of phenol adsorbed at time t, (q_e in mg/g) was calculated using Eq. (1):

$$q_e = \frac{C_0 - C_e}{m_{adsorbant}} \times V_{sol} \quad (1)$$

were V is the volume of the solution (L), and m is the amount of used adsorbent (g).

Kinetic and isotherm models were determined to evaluate the adsorption behavior of the phenol on the prepared hematite, and a variety of models were used to verify the validity of each model. Table S1 (Supplementary Material) lists the description of all used equations. All adsorption experiments were triplicate and averaged.

2.4. Theoretical studies

To unravel the mechanism of adsorption of phenol on hematite, we performed DFT calculations and MD simulations. DFT was achieved by Gaussian 09 package program (Frisch, 2009) using the B3LYP functional (Becke, 1988). The optimization calculations of phenol, α-Fe_2O_3 cluster, and phenol-α-Fe_2O_3 complex were performed employing 6-311++G(d, p) basis set for C, H, and O, and LANL2DZ basis set for Fe atoms. GaussView 5.0.8 program was used to generate molecular structures and visualizations of results (Dennington et al., 2007). The effect of solvent (water) was simulated by using the self-consistent reaction field (SCRF) calculations employing the polarisable continuum model (PCM) (Tapia and Goscinski, 1975). Besides, interactions between phenol and α-Fe_2O_3 were investigated using natural bond orbital (NBO) analysis. The second-order perturbation delocalization energies (E^2) were estimated to determine significant donor–acceptor interactions in the phenol-α-Fe_2O_3 complex.

All molecular dynamics calculations in this work were performed using the Forcite module, which is implemented in Materials Studio software (Studio, n.d.). The used iron oxide model is hexagonal hematite (α-Fe_2O_3) with an R-3c space group. The following lattice constants: a = b = 0.506 nm, c = 1.388 nm, α = β = 90°, and γ = 120° were obtained from the geometrically optimized structure and are in well agreement with experimental values: a = b = 0.504 Å, c = 0.137 5 Å, α = β = 90°, and γ = 120° (Finger and Hazen, 1980). Hematite with an iron terminal was cleaved to (0 0 1) plane, which is the most stable form (Wang et al., 1998; Weiss and Ranke, 2002). The α-Fe_2O_3(0 0 1) surface was simulated by taking a nine atomic layer slab model with the bottom three layers fixed, and a vacuum region, which is placed above the top surface, is set as 12 Å to eliminate unwanted interactions between adjacent slabs. 50 water molecules were used as a model for the solvent effect on the adsorption capacity of phenol on the α-Fe_2O_3(0 0 1) surface. MD simulations were carried out employing the COMPASS force field (Sun, 1998). In the Forcite module, the NVT ensemble with the velocity-Verlet integration algorithm and a time step of 2.0 fs, at temperature T = 30 °C controlled by Nosé-Hoover thermostat were used. Electrostatic interactions were treated by utilizing the Ewald method, and the atom-based cutoff summation method was applied for van der Waals. After the energy minimization, each simulation was performed for 10000 ps in the NVT ensemble to reach the equilibration state. The Phenol-α-Fe_2O_3(0 0 1) interaction energies in vacuum and in water were calculated by Eq. (3) and Eq. (4), respectively:

$$E_{interaction} = E_{total} - \left(E_{surface+H_2O} + E_{Phenol}\right) \quad (2)$$

$$E_{interaction} = E_{total} - \left(E_{surface} + E_{Phenol}\right) \quad (3)$$

where E_{total}denotes the all-system energy, $E_{surface+H_2O}$ and $E_{surface}$ designate, respectively, the α-Fe_2O_3(0 0 1) energy alone

and including water molecules, E_{Phenol}implies the energy of the phenol molecule.

3. Results and discussion

3.1. Characterization of adsorbent

3.1.1. BET analysis and SEM/EDX

Structural properties such as BET specific surface area and pore volume can have significant effects on the performance of adsorbents. These physical properties were determined by the nitrogen gas adsorption measurements. As it is seen from Fig. 1a, the shape of the Nitrogen adsorption–desorption curve contains an H3 hysteresis loop corresponding to plate-like particles or slit-shaped pores, and it is apparent from the curve that it exhibits a type IV shape, according to the classification by IUPAC; typical for mesoporous materials (Gregg and Sing, 1982). Results showed that the BET surface area of the prepared material is 19.4 m^2/g, with an average pore diameter of 188.7 Å and a volume of 0.091 cm^3/g. Horányi and Joó reported a specific surface area of 0.15 m^2/g for a commercial hematite powder (Horányi and Joó, 2002). The larger surface area of our prepared material could enhance the adsorption of the phenol. The surface morphology of the prepared hematite is shown in SEM images (Fig. 1b), which indicates that it has an agglomerate structure. While the EDX analysis (Fig. 2) confirmed the elemental composition of the material under investigation, showing a 68% of iron and 27.34% of oxygen, which is an evidence for the successful formation of the material.

3.1.2. X-Ray diffraction

The X-ray powder diffraction was used to characterize the phase purity and crystalline structure of the prepared hematite sample, as shown in Fig. 3. As can be seen, the sample exhibits eight resolved diffraction peaks at 24.1, 33.1, 35.6, 49.5, 54.1, 58.2, 62 and 64° that can be indexed as (0 1 2), (1 0 4), (1 1 0), (0 2 4), (1 1 6), (2 1 4), (1 1 8) and (4 4 1) reflections. This matched the standard hexagonal α-Fe_2O_3 sample entirely and belonged to the rhomboidal space group in agreement with the standard data (JCPDS No. 86-0550) (Wang et al., 2018). Moreover, no characteristic peaks due to impurities, such as that attributed to α-FeOOH, were detected, indicating the formation of high-purity material and suggesting a

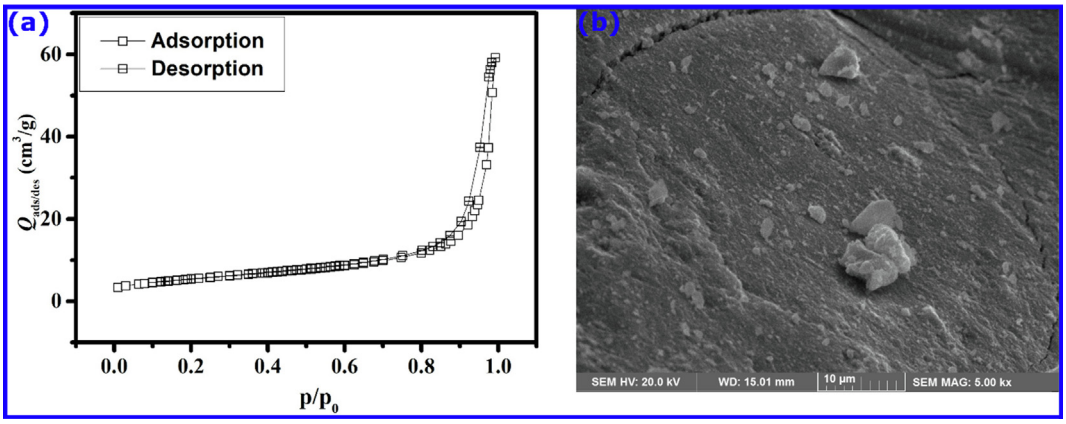

Fig. 1 (a) Nitrogen adsorption and desorption isotherms as a function of relative pressure and (b) SEM micrograph obtained for α-Fe_2O_3.

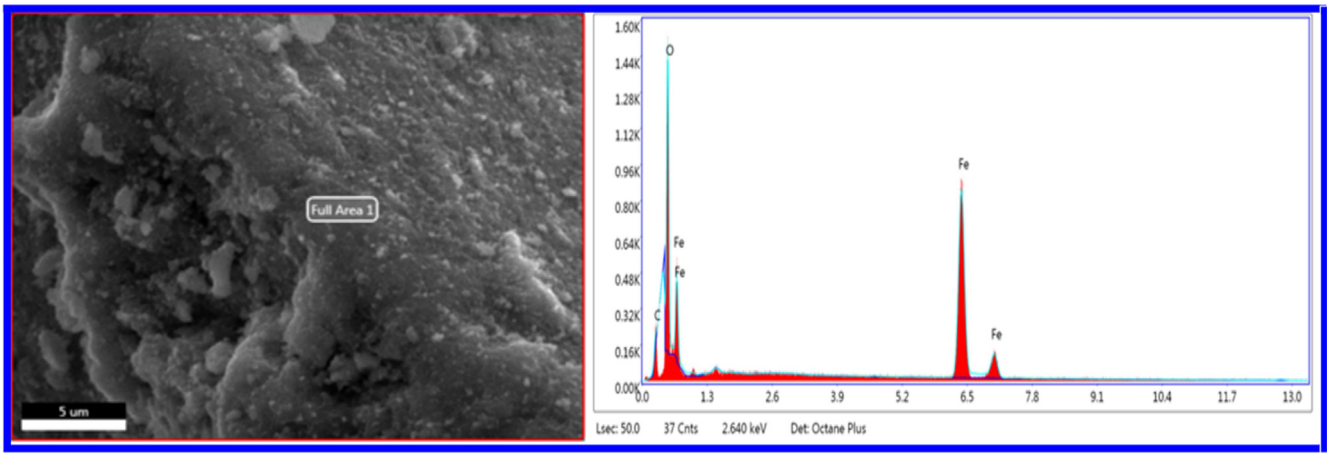

Fig. 2 EDX spectra of the prepared α-Fe_2O_3.

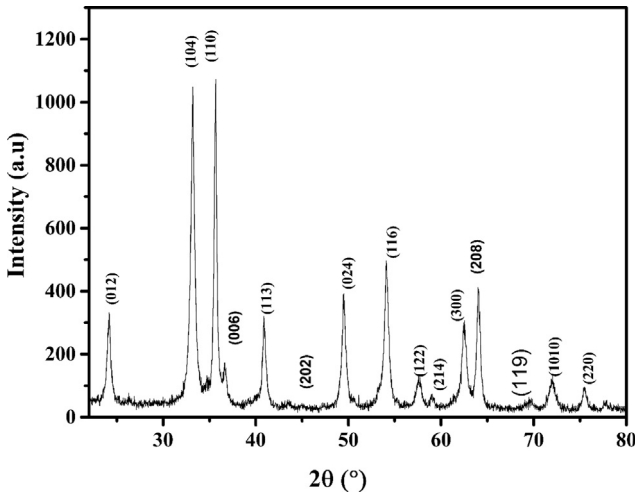

Fig. 3 X-ray diffraction patterns of the prepared α-Fe_2O_3.

thorough phase transformation of goethite (α-FeOOH) to hematite (α-Fe_2O_3) (Yang et al., 2017). Further, peaks are sharper and higher in intensity, which demonstrates the excellent crystallization of hematite particles (Wang et al., 2018; Xia et al., 2016; Yang et al., 2017).

3.2. Adsorption of phenol

3.2.1. Effect of pH

Solution pH affects the adsorption capacity due to its influence on surface properties and the ionization state of the adsorbent as well as ionic forms of phenolic compounds (Quast, 2018). The effect of the solution pH on the ionization degree of absorbate and surface charge of the hematite was studied over a pH range of 2–12. The results described in Fig. 4a revealed that the pH change significantly influenced the adsorption efficiency, which shows a maximum for pH ranging from 2 to ~ 7. When the solution pH is higher than 7, a sudden decrease in the removal efficiency is observed, and then it remains constant over a pH range of 9–12.

The nature of interfacial interactions of mineral/water has a notable influence on the adsorption properties of phenol. Therefore, the pKa of phenol and pH for point of zero charge of the hematite (pH_{zpc}) are decisive factors in determining the nature of the adsorption process. It is well reported in the literature that the pH_{pzc} of hematite is found to be between 6.7 and 9.5 (Cornell and Schwertmann, 2003). In our recent work, we found that the prepared hematite has a pH_{pzc} = 7.1, which indicates that it holds a positive charge at pH below the pH_{zpc} value and a negative charge above it (Dehbi et al., 2020). On the other hand, above the ionization constant (pKa), at pH of 9.89, the phenol exists predominantly as phenolate (Zhu et al., 2005). In this situation, the higher adsorption capacity of phenol at pH = ~2–5 may be due to strong π-π interactions and H-bond interactions between the prepared iron oxide and phenol molecules. Contrariwise, because of homogeneous charge repulsion between phenolates and negatively charged hematite at pH > pH_{pzc}, the adsorption capacity of phenol significantly decreased.

3.2.2. Effects of initial concentration and contact time

We investigated whether the adsorbed quantity of phenol by the iron oxide can be affected by its initial concentration. In Fig. 4b, the amount adsorbed at different initial concentrations of phenol is plotted versus the contact time. Higher phenol concentration increased the iron oxide adsorption capacity, which can be easily seen in Fig. 4b. The increased adsorbed quantity at a higher concentration reflects the strong phenol adsorption on all hematite active sites, and it is attributed to the high adsorption driving force during the adsorption process. Moreover, results show phenol adsorption capacity stabilized at about 10 mg/g at 10^{-3} M of phenol, and, in all cases, it takes up to about 25 min. After this time, hematite's active sites might become saturated, so that a higher exposure time would not further increase the adsorption rate.

3.2.3. Adsorption kinetics

Understanding the kinetics of phenol removal using hematite and evaluation of the rate constants was achieved using pseudo-first-order and pseudo-second-order kinetic models. In the case of comparison between pseudo-first-order and pseudo-second-order models (Fig. 5), results in Table 1 show that the pseudo-second-order model presents a higher R^2 value and a q_e value close to the experimental one, we, therefore, consider this model as the more suitable one to describe

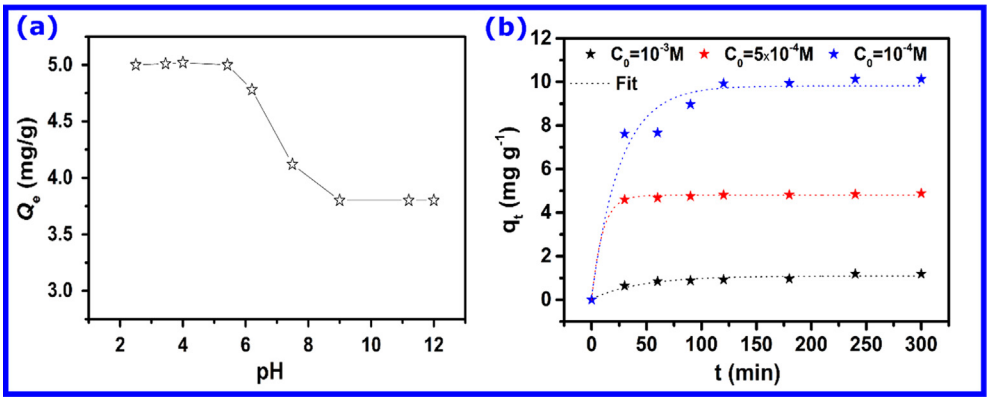

Fig. 4 (a) Effect of the pH on the adsorption of phenol onto hematite and (b) Effect of the contact time on the adsorption of phenol at different concentrations onto hematite.

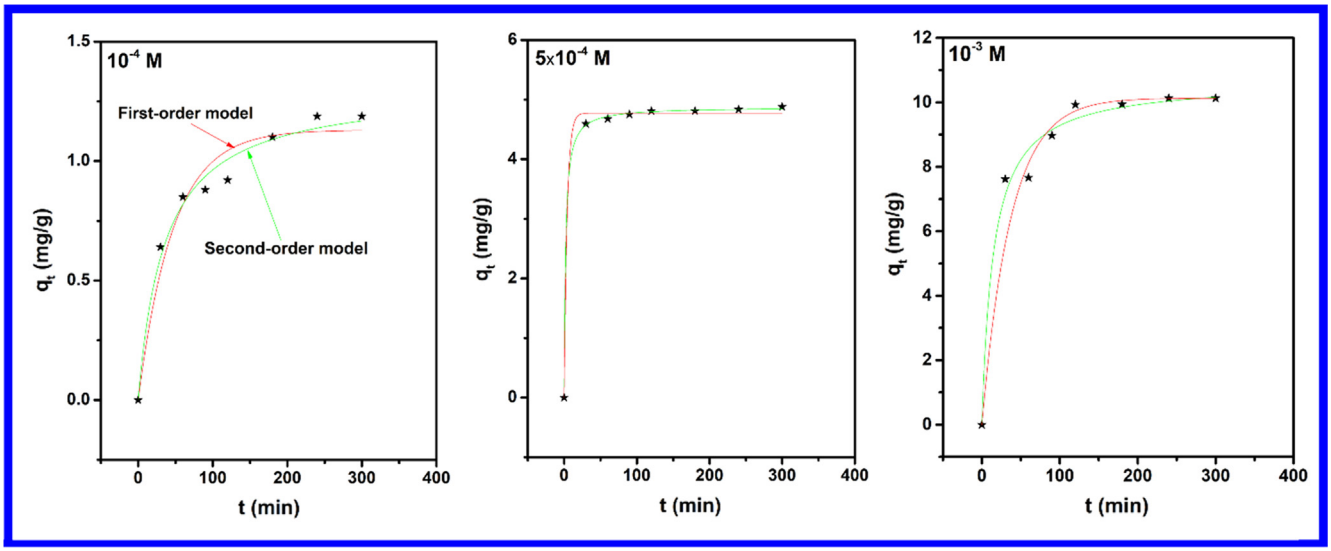

Fig. 5 Pseudo-first order and Pseudo-second order kinetic plots obtained for various concentrations of phenol.

Table 1 Kinetic parameters for phenol adsorption on α-Fe_2O_3.

Model	Parameter	Concentrations		
		10^{-4}	5×10^{-4}	10^{-3}
Pseudo-First ordre	$q_{t,\ exp}$ (mg/g)	1.18	4.88	10.17
	k_1 (min^{-1})	0.02	1.76	2.54
	q_e (mg/g)	1.13	4.76	9.19
	R^2	0.92	0.95	0.76
Pseudo-Second ordre	k_2 (g $mg^{-1}min^{-1}$)	0.019	0.10	0.23
	q_e (mg/g)	1.30	4.87	10.66
	R^2	0.99	0.99	0.99

the adsorption kinetics of phenol on the prepared iron oxide. The applicability of this kinetic model indicates that the rate-determining step may be chemisorption (Oumani et al., 2019). These results would strengthen the idea that π-π interactions could be playing a vital role in the adsorption of phenol.

We note that the intra-particle diffusion model is not interpreted in the present context as it can be applied within very restrictive conditions such as adsorption in a semi-infinite solid and constant liquid phase concentration in the absence of external mass transfer resistance (Lei et al., 2020; Schwaab et al., 2017).

3.2.4. Adsorption isotherm and thermodynamic parameters

Understanding adsorbate-adsorbent interaction is required to understand the adsorption mechanism by which phenol molecules interact with the iron oxide surface (Ba Mohammed et al., 2019; Dehbi et al., 2020). To this end, Freundlich and Langmuir's models were tested with experimentally obtained equilibrium data (at different temperatures) to identify the best-suited model for the adsorption of phenol on iron oxide, and coefficient of determination values along with isothermal parameters are listed in Table 2. Fig. 6 shows that the adsorption capacity for phenol increases with temperature due to the enhancement of the adsorptive interaction between phenol's active sites and hematite. The increase in adsorption with temperature may be attributed to enhancement in the chemical affinity of the phenol to the surface of the adsorbent, leading to some kind of chemical interaction to take place during the adsorption process, which results into increase in adsorption capacity. Based on the coefficient of determination (R^2), the Langmuir isotherm model predicted the equilibrium data for phenol adsorption on iron oxide very well (Fig. 6) and showed a maximum adsorption capacity of 16.17, 17.6, 19.57 and 21.93 mg g^{-1} at 30, 40, 50 and 60 °C. It can, therefore, be expected that homogeneous surfaces would play a more critical role than heterogeneous surfaces during the adsorption process, where the interaction between phenol molecules could be assumed negligible (Ba Mohammed et al., 2019). It should be noted that higher temperatures are not common in industrial effluents and were only considered for analysis of thermodynamic parameters.

Furthermore, to investigate the interaction force in more detail, thermodynamic parameters should be computed. A correct way for calculating thermodynamic parameters is to compute the suitable thermodynamic equilibrium constant (K_e°; dimensionless) at any temperature from the isothermal studies using the following equation (Lima et al., 2019):

$$K_e^\circ = \frac{(1000 \times K_L \text{ molecular weight of adsorbate}) \times [\text{Adsorbate}]^\circ}{\gamma} \quad (4)$$

Table 2 Isotherm parameters for phenol adsorption on α-Fe_2O_3.

Model	Parameters	T (°C)				ΔH° (kJ/mol)	ΔS° (kJ/mol)
		30	40	50	60		
Langmuir Isotherm	q_m (mg/g)	16.17	17.6	19.57	21.93		
	K_L (L/mg)	0.018	0.018	0.020	0.021		
	R^2	0.98	0.98	0.95	0.98	3.96	75.00
	ΔG° (kJ/mol)	−18.75	−19.34	−20.24	−21.01		
Freundlich Isotherm	K_F (mg/g)	1.78	1.89	2.25	2.81		
	1/n	0.29	0.30	0.32	0.33		
	R^2	0.87	0.90	0.91	0.97		

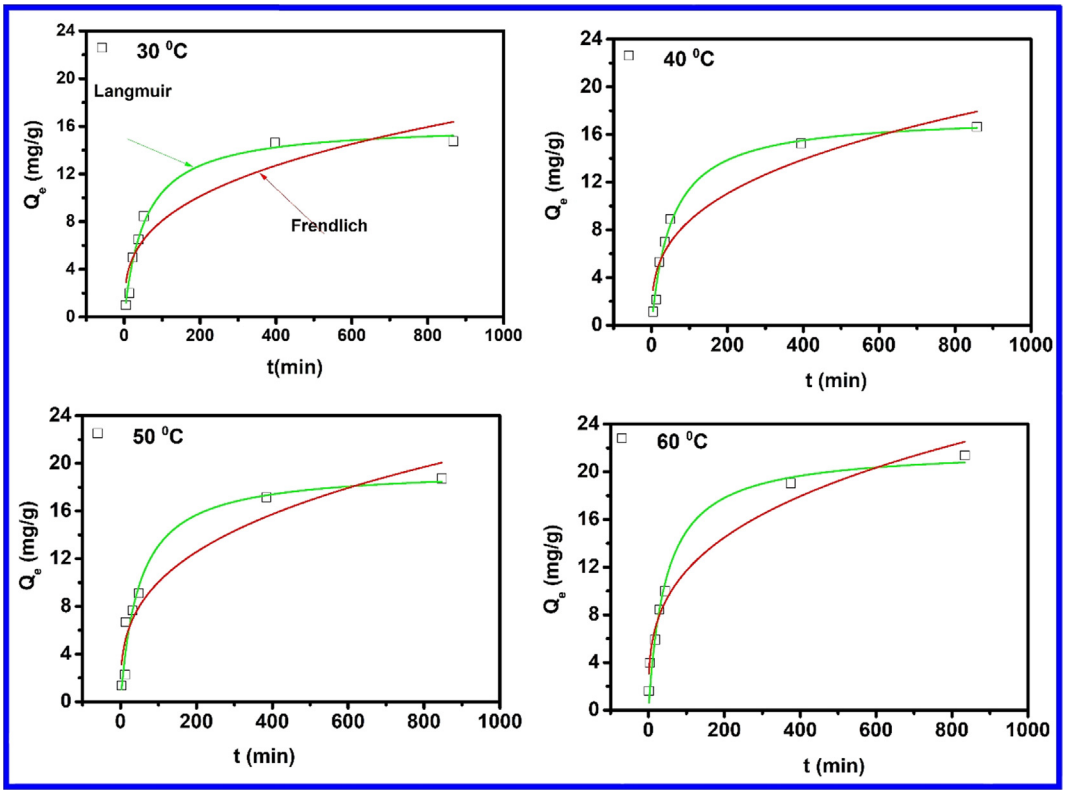

Fig. 6 Adsorption isotherms for phenol on α-Fe_2O_3 at different temperatures.

where K_L is the isotherm constant, [Adsorbate]° is the standard concentration of the adsorbate (1 mol L^{-1}) (Chang and John W Thoman, 2014) and γ is the coefficient of activity of adsorbate (dimensionless) which can be considered as unity (Atkins and de Paula, 2009). The free energy change (ΔG°), enthalpy change (ΔH°), and entropy change (ΔS°) were determined using the following equations (Lima et al., 2019):

$$\Delta G^\circ = -RT\ln(K_e^\circ) \quad (5)$$

$$\ln(K_e^\circ) = \frac{-\Delta H^\circ}{R} \times \frac{1}{T} + \frac{\Delta S^\circ}{R} \quad (6)$$

where R is the universal gas constant (8.314 J K^{-1} mol^{-1}), and T is the temperature (K).

Fig. 7 shows the plot of ln (K_e°) vs. 1/T; a straight line was obtained with a good regression coefficient value, and thermodynamic parameters are listed in Table 2. We could show that the adsorption capacity increased gradually with increasing temperature. Results also showed negative values of ΔG°_{ads}, which expresses the feasibility and spontaneous nature of phenol adsorption onto prepared hematite (Rahman and Sathasivam, 2015). Also, positive values of change in enthalpy ΔH°_{ads} and of change in entropy ΔS°_{ads} show that the adsorption is endothermic and random at the hematite/-solution interphase (Adeyemo et al., 2017; Rahman and Sathasivam, 2015).

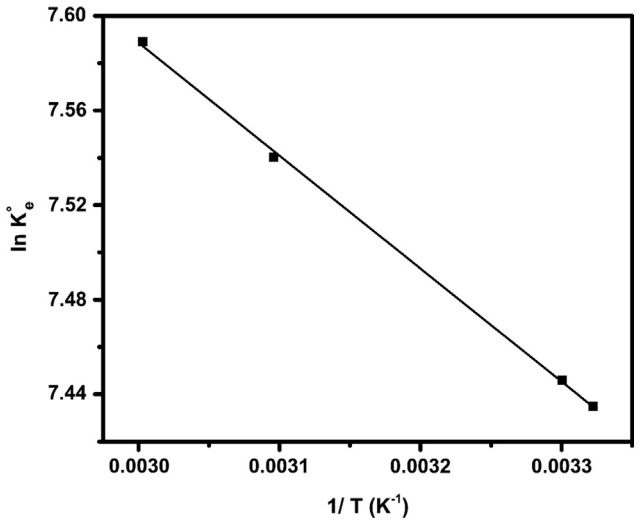

Fig. 7 ln K_e° vs. 1/T plot for phenol adsorption on α-Fe_2O_3.

3.3. DFT calculations

3.3.1. Phenol-α-Fe_2O_3 complex

To gain theoretical insights that could support and complement experimental results, we performed DFT calculations of the interaction between the phenol molecule and hematite cluster. For easy calculation and interpretation of results, a simple α-Fe_2O_3 monomer was considered. Fig. 8 represents the optimized structures of the Phenol-α-Fe_2O_3 complex. Results reveal the formation of two bonds Fe5-C11 and Fe1-C9 with bond lengths of 2.12601 and 2.10239, respectively (Table 3). This indicates that π–π interactions are most likely

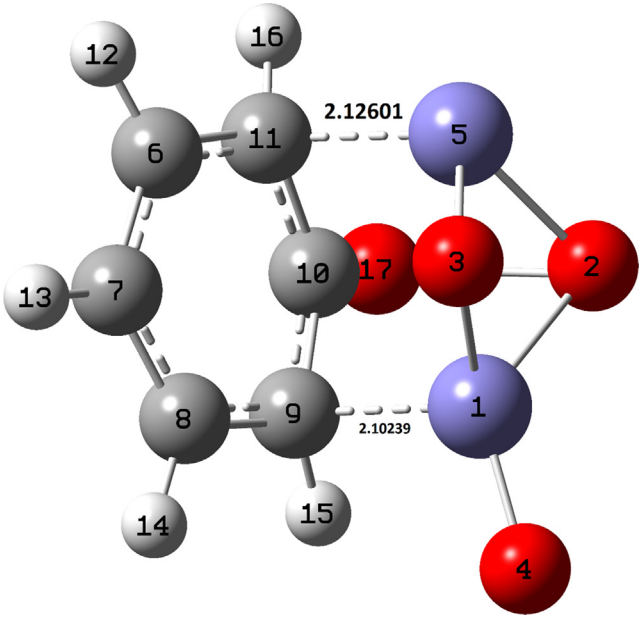

Fig. 8 Optimized structure of the phenol-α-Fe_2O_3 complex in aqueous solution calculated at the CPCM/B3LYP with LANL2DZ basis set for Fe atoms and 6–311 + + G(d,p) basis set for other atoms.

Table 3 Theoretical geometric parameters for Phenol-hematite complex calculated at the B3LYP with LANL2DZ basis set for the Fe atoms and the 6-311 + + G(d,p) basis set for C, H, and O atoms; (Å).

Bond	Bond length
Fe1—O3	1.80555
Fe1—O2	1.91154
Fe1—O4	1.56810
Fe5—O3	1.75900
Fe5—O2	1.90707
C10—O17	1.26566
C10—C9	1.49649
C9—C8	1.43406
C8—C7	1.40753
C7—C6	1.40632
C6—C11	1.43492
C11—C10	1.48837
Fe5—C11	2.12601
Fe1—C9	2.10239
O17—H18	2.29134
C9—H15	1.09167
C8—H14	1.08802
C7—H13	1.08435
C6—H12	1.08970
C11—H16	1.09439

a significant factor in regulating the adsorption capacity. Further, the elongation of O17-H18 is mainly an indication of hydrogen bond formation between hematite and phenol molecule (Singh and Singh, 2015; Sreenath et al., 2018). Phenol-hematite interactions will be addressed later in more detail using NBO analysis.

The energies of the frontier molecular orbitals, i.e., highest occupied molecular orbital (HOMO) and lowest unoccupied molecular orbital (LUMO) are important electronic parameters to investigate the reactivity and stability of the phenol-α-Fe_2O_3 complex. The HOMO and LUMO energies and their gaps for phenol, hematite, and phenol-α-Fe_2O_3 complex are listed in Table 4. Inspection of results reveals that adsorption of phenol molecule induced a significant change in HOMO and LUMO energies. Such an effect could be attributed to a chemisorption type of adsorption (Rad et al., 2017). Besides, we noticed an increase in the energy gap from 2.723 (hematite) to 3.209 (phenol-α-Fe_2O_3 complex), suggesting that the formed phenol-α-Fe_2O_3 complex is more stable than isolated hematite (Lgaz et al., 2019).

Table 4 HOMO, LUMO and energy gap values (in eV) of phenol, hematite and their resultant complex calculated at the B3LYP with LANL2DZ basis set for the Fe atoms and the 6-311 + + G(d,p) basis set for C, H, and O atoms.

System	E_{HOMO}	E_{LUMO}	ΔE
Phenol	−6.264	−0.384	5.879
Hematite	−7.248	−4.525	2.723
Phenol-hematite	−6.351	−3.142	3.209

3.3.2. NBO analysis

NBO analysis is an efficient way to elucidate the charge transfer interactions, donor–acceptor interactions, and charge distribution (Xavier and Gobinath, 2012). It can be used as a convenient means to investigate the relationship between the donor (filled orbitals) and acceptor (virtual orbitals) (Demircioğlu et al., 2015). The stabilization energy (E^2), which can be obtained from the second-order Fock-matrix analysis, is directly proportional to the NBO interaction intensities. Therefore, we could say that the strength of the electron transfer process between an electron donor and an electron acceptor is more pronounced when the stabilization energy is higher (Demircioğlu et al., 2015). Herein, the NBO analysis of the phenol-α-Fe_2O_3 complex was calculated to investigate the electron donor and acceptor properties of the formed complex. Donor-acceptor interactions having high stabilization energy are listed in Table S2 (SM). Evaluation of these results reveals that multiple types of donor–acceptor interactions play a role in the stabilization of the formed complex. In the case of the donating electrons from the phenol molecule to the hematite atoms, the highest contributions were from the lone pairs of electrons on C9 and C11 atoms. The significant interactions are from LP (1) C9 to LP*(3)Fe1, LP*(5)Fe1, and BD*(2) Fe1 - O4 with stabilization energies (E^2) equal to 201.84, 65.44, and 65.06 kJ/mol, respectively. And from LP (1) C11 to LP*(4)Fe5, LP*(5)Fe5 and LP*(6)Fe5 with E^2 equal to 553.29, 80.16 and 70.66 kcal/mol, respectively. These results match what we found previously based on geometry optimization and indicate the crucial role of electron-density donation in the adsorption process.

Besides its ability to donate electrons, the phenol molecule could also accept electrons from hematite atoms through electron-back-donation. As the results in Table S2, we could see that the most significant interactions occur between lone pairs of electrons on iron atoms and Rydberg non-Lewis orbitals of the phenol molecule. Interesting interactions having the highest stabilization energy are from LP*(3)Fe1 to RY*(2) C7, RY*(2) C8, RY*(3) C9, RY*(2) C10, and RY*(3) C10 leading to stabilization energies of 89.54, 162.76, 116.35, 91.58, 90.83 kJ/mol, respectively.

Furthermore, NBO analysis indicates H-bond formation between hematite atoms and the phenol molecule. Results revealed that the dominant donor–acceptor charge-transfer interactions occur between the antibonding lone pair of iron atoms (LP*(5)Fe5) and σ*(1) C11 - H16 and σ*(1) C9 - H15 with stabilization energy of 50.16 and 21.88 kJ/mol, respectively, and between σ(1) C9 - H15 and LP*(3)Fe1 with stabilization energy of 37.53 kJ/mol. These hydrogen bonds could additionally facilitate the adsorption of the phenol on the hematite surface.

3.4. Molecular dynamics simulations

Theoretical modelling is a powerful tool to bridge the gap between experimental data and macroscopic theories and to understand physical phenomena at the atomistic level (Guediri et al., 2020; Han et al., 2019). In this section, we used molecular dynamics (MD) simulations to, theoretically, explore the mechanism of adsorption of the phenol molecule on the hematite (α-Fe_2O_3) surface. The solution environment plays a primordial role in enhancing or diminishing the adsorption capacity of phenol due to its influence on adsorbate-adsorbent interactions. Therefore, simulations were carried out in both vacuum and the presence of solvent (water molecules), in an attempt to mimic the effect of the solvent as much as possible. Snapshots of the most stable configuration of phenol molecules on hematite (0 0 1) surface in both mediums are shown in Fig. 9. We note that the phenol molecules were flexible, could lie, twist, or float on the α-Fe_2O_3(0 0 1) surface. It is interesting to observe that phenol molecule in both

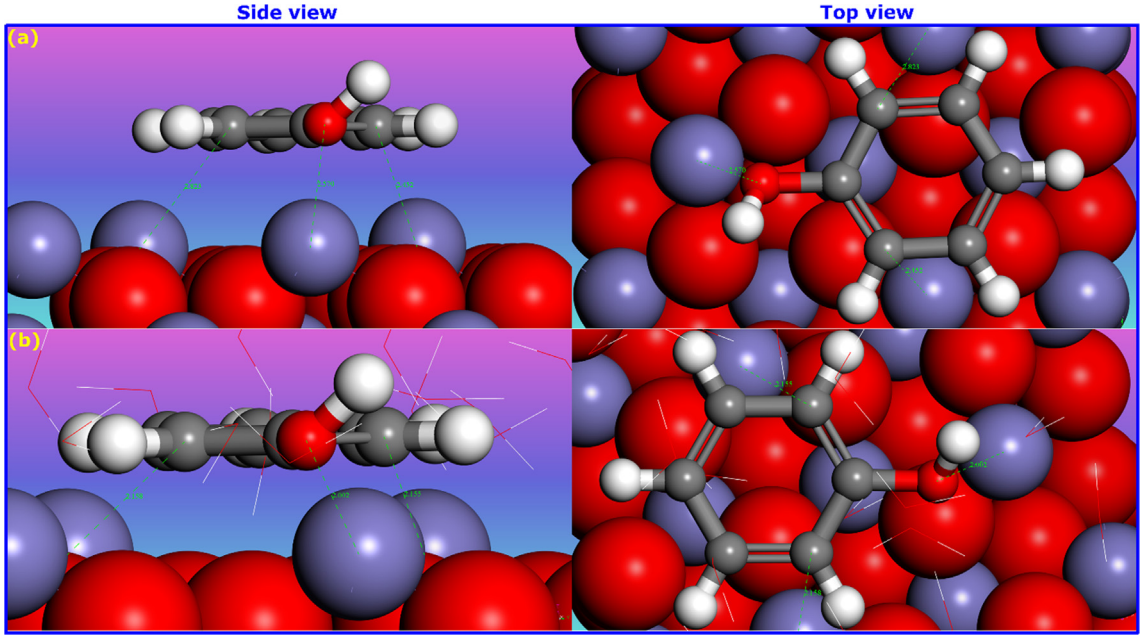

Fig. 9 Configurations of phenol molecules adsorption on α-Fe_2O_3(0 0 1) surface obtained by MD simulations. (a) In vacuum and (b) In the presence of water molecules.

Table 5 Literature results of the adsorption of phenol by different adsorbents.

Adsorbent	Adsorption capacity (mg g^{-1})	Reference
Borassus flabellifer fruit husk activated carbon (Pyrolysis)	13.97	(Priya and Sureshkumar, 2020)
Borassus flabellifer fruit husk activated carbon (H2SO4 activation)	13.42	(Priya and Sureshkumar, 2020)
Microorganism P. putida and acid-modified CESEP/ZIF-8	5.96	(Dong et al., 2020)
Rice Husk	7.89	(Mandal et al., 2019)
Acid modified bentonite	6.8	(Ahmadi and Igwegbe, 2018)
Iron impregnated A/C	2.0	(M. Ge et al., 2019)
Tea waste biomass	9.49	(Gupta and Balomajumder, 2015)
Zeolite	4.31	(Cheng et al., 2016)
Solvent extraction	3.45	(Yang et al., 2006)
magnetic iron oxide nanopowder (MNM)	13.51	(Mihoc et al., 2014)
Fe3O4@GO on silica sand	0.0731	(Mehmanravesh et al., 2019)
Methyl acrylic acid (MAA)-coated iron oxide nanoparticles (NPs)	950	(Yoon et al., 2016)
Uncoated iron oxide nanoparticles (NPs)	550	(Yoon et al., 2016)
α-Fe_2O_3	16.17	This work

vacuum and solvent phases is found to lie parallel to the hematite surface, with more close contact with the hematite surface in the presence of water molecules. The phenol molecule adsorbed on the hematite surface in the presence of solvent exhibits binding energy of −79.83 kJ/mol, which is larger than that in a vacuum (-55.73 kJ/mol).

Furthermore, vertical distances (α-Fe_2O_3(0 0 1)…C9 = 2.155 Å, α-Fe_2O_3(0 0 1)…C11 = 2.158 Å, and α-Fe_2O_3(0 0 1)…O17 = 2.002 Å) were found for phenol in solvent compared to that in a vacuum, which has interaction distances of (α-Fe_2O_3(0 0 1)…C9 = 2.452 Å, α-Fe_2O_3(0 0 1)…C11 = 2.823 Å, and α-Fe_2O_3(0 0 1)…O17 = 2.570 Å). A close vertical distance in both cases reveals that π-π interactions may potentially play a significant role in the interaction between the phenol molecule and the hematite surface. Comparing with that in the solvent, we can see that the interaction distance in a vacuum is large, and thus π-π interactions are significantly weakened. Interestingly, close interaction between phenol molecule and hematite surface in the presence of water molecules implies that water-bridged H-bonds have potentially a crucial role in controlling the adsorption capacity along with π–π interactions.

Overall, it seems that simulations results meet our expectations that π-π interactions, along with water-bridged H-bonds, are playing a significant role in enhancing the adsorption of phenol molecules on the hematite surface. In the experimental results, we showed that adsorption capacity was higher in the pH range of 2–7, which means that the interaction occurs in a broad pH range between neutral phenol molecule and positively charged hematite, with a minimal contribution of interactions with near-neutral hematite; considering the pH_{pzc} of hematite. In this situation, the following reactions between phenol and hematite surface can be suggested (Bandara et al., 2001):

$$Ph + F_eOH_2^+ \rightarrow FePh + H_2O + H^+ \quad (7)$$

$$Ph + F_eOH \rightarrow FePh + H_2O \quad (8)$$

Herein, reaction (7) is particularly important, bearing in mind that high adsorption capacity is obtained at an acid pH. In alkaline solution (pH > pKa), there is expected a strong electrostatic repulsion between deprotonated phenol molecule and negatively charged hematite surface, and therefore the adsorption affinity could be significantly decreased.

3.5. Comparison with other adsorbents

Table 5 compares the adsorption capacities for phenol on different kinds of adsorbents reported in the literature. Presumedly, the difference in properties and operating conditions may cause different results. These differences are evident in the results reported in Table 5, which indicates that adsorbent's properties have a significant effect on its efficacy. Taking all this into account, it seems that the hematite used in this study is an exciting candidate to be an effective adsorbent for phenol removal. Results in Table 5 indicate that it shows a high adsorption capacity compared to a wide range of adsorbents. However, the adsorption capacity of the present hematite would be much higher, especially if it is adequately modified with suitable materials. For instance, as can be seen, the adsorption capacity of Methyl acrylic acid (MAA)-coated iron oxide nanoparticles (NPs) is remarkably higher than that of our prepared material.

4. Conclusion

In this paper, a hematite iron oxide (α-Fe_2O_3) has been prepared from an aqueous solution of iron nitrate by the precipitation method, and its adsorption capacity for phenol removal from the aqueous system was exhaustively examined and discussed from theoretical and experimental perspectives. Benefitting from its structural advantages such as large surface area, the prepared material displays excellent adsorption performance. Obtained results show that operating parameters influence on adsorption capacity with initial concentration playing a significant role. The adsorption kinetics data are matched nicely with the pseudo-second-order model, and results show that adsorption behavior of phenol on the iron oxide is mainly controlled by chemisorption. This adsorption follows the Langmuir model, which suggests monolayer adsorption, and it is spontaneous and endothermic. Theoretical investigations by DFT and MD simulations, support the conclusions from experimental results and confirm that π-π interactions, along with water-bridged H-bonds, have a significant role in enhancing the adsorption of phenol molecules on the hematite surface.

Declaration of Competing Interest

The authors declare that they have no known competing financial interests or personal relationships that could have appeared to influence the work reported in this paper.

Acknowledgments

This work was supported by the Institute of Research and Consulting Studies at Umm Al-Qura University (Grant Code. 19-SCI-1-01-0003).

Appendix A. Supplementary material

Supplementary data to this article can be found online at https://doi.org/10.1016/j.arabjc.2020.03.026.

References

Adeyemo, A.A., Adeoye, I.O., Bello, O.S., 2017. Adsorption of dyes using different types of clay: a review. Appl. Water Sci. 7, 543–568.

Ahmadi, S., Igwegbe, C.A., 2018. Adsorptive removal of phenol and aniline by modified bentonite: adsorption isotherm and kinetics study. Appl. Water Sci. 8, 170.

Ahmed, S.M., El-Dib, F.I., El-Gendy, N.Sh., Sayed, W.M., El-Khodary, M., 2016. A kinetic study for the removal of anionic sulphonated dye from aqueous solution using nano-polyaniline and Baker's yeast. Arab. J. Chem. 9, S1721–S1728. https://doi.org/10.1016/j.arabjc.2012.04.049.

Ali, M.E.A., 2018. Synthesis and adsorption properties of chitosan-CDTA-GO nanocomposite for removal of hexavalent chromium from aqueous solutions. Arab. J. Chem. 11, 1107–1116. https://doi.org/10.1016/j.arabjc.2016.09.010.

Arumugam, N., Chelliapan, S., Kamyab, H., Thirugnana, S., Othman, N., Nasri, N.S., 2018. Treatment of wastewater using seaweed: A review. Int. J. Environ. Res. Public. Health 15, 2851. https://doi.org/10.3390/ijerph15122851.

Atkins, P., de Paula, J., 2009. Physical Chemistry. W. H Freeman, New York.

Ba Mohammed, B., Yamni, K., Tijani, N., Alrashdi, A.A., Zouihri, H., Dehmani, Y., Chung, I.-M., Kim, S.-H., Lgaz, H., 2019. Adsorptive removal of phenol using faujasite-type Y zeolite: Adsorption isotherms, kinetics and grand canonical Monte Carlo simulation studies. J. Mol. Liq. 296, 111997. https://doi.org/10.1016/j.molliq.2019.111997.

Bandara, J., Tennakone, K., Kiwi, J., 2001. Surface mechanism of molecular recognition between aminophenols and iron oxide surfaces. Langmuir 17, 3964–3969. https://doi.org/10.1021/la001411w.

Banerjee, S., Chattopadhyaya, M.C., 2017. Adsorption characteristics for the removal of a toxic dye, tartrazine from aqueous solutions by a low cost agricultural by-product. Arab. J. Chem. 10, S1629–S1638. https://doi.org/10.1016/j.arabjc.2013.06.005.

Becke, A.D., 1988. Density-functional exchange-energy approximation with correct asymptotic behavior. Phys. Rev. A 38, 3098.

Chang, R., John W Thoman, J., 2014. Physical Chemistry for the Chemical Sciences.

Chatterjee, D., Dasgupta, S., 2005. Visible light induced photocatalytic degradation of organic pollutants. J. Photochem. Photobiol. C Photochem. Rev. 6, 186–205.

Cheng, W.P., Gao, W., Cui, X., Ma, J.H., Li, R.F., 2016. Phenol adsorption equilibrium and kinetics on zeolite X/activated carbon composite. J. Taiwan Inst. Chem. Eng. 62, 192–198.

Cornell, R.M., Schwertmann, U., 2003. The Iron Oxides: Structure, Properties, Reactions, Occurrences and Uses. John Wiley & Sons.

Das, M.R., Bordoloi, D., Borthakur, P.C., Mahiuddin, S., 2005. Kinetics and adsorption of benzoate and salicylate at the natural hematite–water interface. Colloids Surf. Physicochem. Eng. Asp. 254, 49–55. https://doi.org/10.1016/j.colsurfa.2004.11.025.

Dehbi, A., Dehmani, Y., Omari, H., Lammini, A., Elazhari, K., Abdallaoui, A., 2020. Hematite iron oxide nanoparticles (α-Fe2O3): Synthesis and modelling adsorption of malachite green. J. Environ. Chem. Eng. 8, 103394. https://doi.org/10.1016/j.jece.2019.103394.

Demircioğlu, Z., Kaştaş, Ç.A., Büyükgüngör, O., 2015. Theoretical analysis (NBO, NPA, Mulliken Population Method) and molecular orbital studies (hardness, chemical potential, electrophilicity and Fukui function analysis) of (E)-2-((4-hydroxy-2-methylphenylimino)methyl)-3-methoxyphenol. J. Mol. Struct. 1091, 183–195. https://doi.org/10.1016/j.molstruc.2015.02.076.

Dennington, R., Keith, T., Millam, J., 2007. GaussView, Version 4.1. 2. Semichem Inc Shawnee Mission KS.

Dong, R., Chen, D., Li, N., Xu, Q., Li, H., He, J., Lu, J., 2020. Removal of phenol from aqueous solution using acid-modified Pseudomonas putida-sepiolite/ZIF-8 bio-nanocomposites. Chemosphere 239, 124708.

Dzade, N., Roldan, A., de Leeuw, N., 2014. A density functional theory study of the adsorption of benzene on hematite (α-Fe2O3) surfaces. Minerals 4, 89–115.

Elsagh, A., Moradi, O., Fakhri, A., Najafi, F., Alizadeh, R., Haddadi, V., 2017. Evaluation of the potential cationic dye removal using adsorption by graphene and carbon nanotubes as adsorbents surfaces. Arab. J. Chem. 10, S2862–S2869. https://doi.org/10.1016/j.arabjc.2013.11.013.

Essandoh, M., Garcia, R.A., 2018. Efficient removal of dyes from aqueous solutions using a novel hemoglobin/iron oxide composite. Chemosphere 206, 502–512. https://doi.org/10.1016/j.chemosphere.2018.04.182.

Finger, L.W., Hazen, R.M., 1980. Crystal structure and isothermal compression of Fe2O3, Cr2O3, and V2O3 to 50 kbars. J. Appl. Phys. 51, 5362–5367.

Frisch, A., 2009. gaussian 09W Reference. Wallingford USA 25p.

Gautam, A., Rawat, S., Verma, L., Singh, J., Sikarwar, S., Yadav, B. C., Kalamdhad, A.S., 2018. Green synthesis of iron nanoparticle from extract of waste tea: An application for phenol red removal from aqueous solution. Environ. Nanotechnol. Monit. Manag. 10, 377–387. https://doi.org/10.1016/j.enmm.2018.08.003.

Ge, M., Wang, X., Du, M., Liang, G., Hu, G., SM, J.A., 2019. Adsorption analyses of phenol from aqueous solutions using magadiite modified with organo-functional groups: Kinetic and equilibrium studies. Materials 12, 96.

Ge, Y.-L., Zhang, Y.-F., Yang, Y., Xie, S., Liu, Y., Maruyama, T., Deng, Z.-Y., Zhao, X., 2019b. Enhanced adsorption and catalytic degradation of organic dyes by nanometer iron oxide anchored to single-wall carbon nanotubes. Appl. Surf. Sci. 488, 813–826. https://doi.org/10.1016/j.apsusc.2019.05.221.

Gregg, S., Sing, K., 1982. W. Adsorption, Surface Area and Porosity. Lond. Acad. Press, pp. 195–197.

Guediri, A., Bouguettoucha, A., Chebli, D., Chafai, N., Amrane, A., 2020. Molecular dynamic simulation and DFT computational studies on the adsorption performances of methylene blue in aqueous solutions by orange peel-modified phosphoric acid. J. Mol. Struct. 1202, 127290. https://doi.org/10.1016/j.molstruc.2019.127290.

Gupta, A., Balomajumder, C., 2015. Simultaneous removal of Cr (VI) and phenol from binary solution using Bacillus sp. immobilized onto tea waste biomass. J. Water Process Eng. 6, 1–10.

Han, Y., Ma, T., Chen, F., Li, W., Zhang, J., 2019. Supercritical water gasification of naphthalene over iron oxide catalyst: A ReaxFF molecular dynamics study. Int. J. Hydrog. Energy 44, 30486–30498. https://doi.org/10.1016/j.ijhydene.2019.09.215.

Harris, R.A., 2019. Chemotherapy drug temozolomide adsorbed onto iron-oxide (Fe3O4) nanoparticles as nanocarrier: A simulation

study. J. Mol. Liq. 288, 111084. https://doi.org/10.1016/j.molliq.2019.111084.
Horányi, G., Joó, P., 2002. Some peculiarities in the specific adsorption of phosphate ions on hematite and γ-Al2O3 as reflected by radiotracer studies. J. Colloid Interface Sci. 247, 12–17.
Hosseini, J., Zare, E.N., Ajloo, D., 2019. Experimental and theoretical calculation investigation on effective adsorption of lead(II) onto poly(aniline-co-pyrrole) nanospheres. J. Mol. Liq. 296, 111789. https://doi.org/10.1016/j.molliq.2019.111789.
Hwang, H., Sahin, O., Choi, J.W., 2017. Manufacturing a super-active carbon using fast pyrolysis char from biomass and correlation study on structural features and phenol adsorption. RSC Adv. 7, 42192–42202.
Hwang, Y.S., Liu, J., Lenhart, J.J., Hadad, C.M., 2007. Surface complexes of phthalic acid at the hematite/water interface. J. Colloid Interface Sci. 307, 124–134. https://doi.org/10.1016/j.jcis.2006.11.020.
Kuntail, J., Jain, Y.M., Shukla, M., Sinha, I., 2019. Adsorption mechanism of phenol, p-chlorophenol, and p-nitrophenol on magnetite surface: A molecular dynamics study. J. Mol. Liq. 288, 111053. https://doi.org/10.1016/j.molliq.2019.111053.
Kuznetsov, M.L., Rocha, B.G., Pombeiro, A.J., Shul'pin, G.B., 2015. Oxidation of olefins with hydrogen peroxide catalyzed by bismuth salts: A mechanistic study. ACS Catal. 5, 3823–3835.
Lei, Y., Huang, Q., Gan, D., Huang, H., Chen, J., Deng, F., Liu, M., Li, X., Zhang, X., Wei, Y., 2020. A novel one-step method for preparation of sulfonate functionalized nanodiamonds and their utilization for ultrafast removal of organic dyes with high efficiency: Kinetic and isotherm studies. J. Environ. Chem. Eng. 8, 103780.
Lgaz, H., Chung, I.-M., Salghi, R., Ali, I.H., Chaouiki, A., El Aoufir, Y., Khan, M.I., 2019. On the understanding of the adsorption of Fenugreek gum on mild steel in an acidic medium: Insights from experimental and computational studies. Appl. Surf. Sci. 463, 647–658. https://doi.org/10.1016/j.apsusc.2018.09.001.
Li, B., Liu, S., Guo, J., Zhang, L., 2018. Interaction between low rank coal and kaolinite particles: A DFT simulation. Appl. Surf. Sci. 456, 215–220.
Lima, E.C., Hosseini-Bandegharaei, A., Moreno-Pirajᴀn, J.C., Anastopoulos, I., 2019. A critical review of the estimation of the thermodynamic parameters on adsorption equilibria. Wrong use of equilibrium constant in the Van't Hoof equation for calculation of thermodynamic parameters of adsorption. J. Mol. Liq. 273, 425–434.
Mandal, A., Mukhopadhyay, P., Das, S.K., 2019. The study of adsorption efficiency of rice husk ash for removal of phenol from wastewater with low initial phenol concentration. SN Appl. Sci. 1, 192.
Mehmanravesh, S., Farhadi, K., Torabian, A., Hessam Hassani, A., 2019. Fe3O4@ GO on silica sand as an efficient and economical adsorbent; Typical application for removal of phenol and 2, 4-dichlorophenol from water samples. Water Environ. Res. 91, 1509–1517.
Mihoc, G., Ianoş, R., Păcurariu, C., 2014. Adsorption of phenol and p-chlorophenol from aqueous solutions by magnetic nanopowder. Water Sci. Technol. 69, 385–391.
Milagres, J.L., Bellato, C.R., Ferreira, S.O., de Moura Guimarães, L., 2020. Preparation and evaluation of hydrocalumite-iron oxide magnetic intercalated with dodecyl sulfate for removal of agrichemicals. J. Environ. Manage. 255, 109845. https://doi.org/10.1016/j.jenvman.2019.109845.
Novikov, A.S., Kuznetsov, M.L., Pombeiro, A.J., Bokach, N.A., Shul'pin, G.B., 2013. Generation of HO• radical from hydrogen peroxide catalyzed by aqua complexes of the group III metals [M(H2O) n] 3 + (M = Ga, In, Sc, Y, or La): a theoretical study. ACS Catal. 3, 1195–1208.
Novikov, A.S., Kuznetsov, M.L., Rocha, B.G.M., Pombeiro, A.J.L., Shul'pin, G.B., 2016. Oxidation of olefins with H2O2 catalysed by salts of group III metals (Ga, In, Sc, Y and La): epoxidation versus hydroperoxidation. Catal. Sci. Technol. 6, 1343–1356. https://doi.org/10.1039/C5CY01367D.
Oumani, A., Mandi, L., Berrekhis, F., Ouazzani, N., 2019. Removal of Cr3 + from tanning effluents by adsorption onto phosphate mine waste: Key parameters and mechanisms. J. Hazard. Mater. 378, 120718. https://doi.org/10.1016/j.jhazmat.2019.05.111.
Parfitt, R.L., Farmer, V.C., Russell, J.D., 1977. Adsorption on hydrous oxides I. oxalate and benzoate on goethite. J. Soil Sci. 28, 29–39. https://doi.org/10.1111/j.1365-2389.1977.tb02293.x.
Pathania, D., Sharma, S., Singh, P., 2017. Removal of methylene blue by adsorption onto activated carbon developed from Ficus carica bast. Arab. J. Chem. 10, S1445–S1451. https://doi.org/10.1016/j.arabjc.2013.04.021.
Priya, D.S., Sureshkumar, M.V., 2020. Synthesis of Borassus flabellifer fruit husk activated carbon filter for phenol removal from wastewater. Int. J. Environ. Sci. Technol. 17, 829–842.
Quast, K., 2018. Direct measurement of oleate adsorption on hematite and its consequences for flotation. Miner. Eng. 118, 122–132. https://doi.org/10.1016/j.mineng.2017.12.011.
Rad, A.S., Sani, E., Binaeian, E., Peyravi, M., Jahanshahi, M., 2017. DFT study on the adsorption of diethyl, ethyl methyl, and dimethyl ethers on the surface of gallium doped graphene. Appl. Surf. Sci. 401, 156–161.
Rahman, Md.S., Sathasivam, K.V., 2015. Heavy metal adsorption onto Kappaphycus sp. from aqueous solutions: the use of error functions for validation of isotherm and kinetics models. BioMed Res. Int. 2015. https://doi.org/10.1155/2015/126298.
Sartape, A.S., Mandhare, A.M., Jadhav, V.V., Raut, P.D., Anuse, M.A., Kolekar, S.S., 2017. Removal of malachite green dye from aqueous solution with adsorption technique using Limonia acidissima (wood apple) shell as low cost adsorbent. Arab. J. Chem. 10, S3229–S3238. https://doi.org/10.1016/j.arabjc.2013.12.019.
Schwaab, M., Steffani, E., Barbosa-Coutinho, E., Júnior, J.B.S., 2017. Critical analysis of adsorption/diffusion modelling as a function of time square root. Chem. Eng. Sci. 173, 179–186.
Shen, Y., Zhang, N., Fu, Y., 2019. Synthesis of high-performance hierarchically porous carbons from rice husk for sorption of phenol in the gas phase. J. Environ. Manage. 241, 53–58. https://doi.org/10.1016/j.jenvman.2019.04.012.
Singh, R.K., Singh, A.K., 2015. Synthesis, molecular structure, spectral analysis, natural bond order and intramolecular interactions of 2-acetylpyridine thiosemicarbazone: A combined DFT and AIM approach. J. Mol. Struct. 1094, 61–72. https://doi.org/10.1016/j.molstruc.2015.03.064.
Somasekhara Reddy, M.C., Nirmala, V., Ashwini, C., 2017. Bengal Gram Seed Husk as an adsorbent for the removal of dye from aqueous solutions – Batch studies. Arab. J. Chem. 10, S2554–S2566. https://doi.org/10.1016/j.arabjc.2013.09.029.
Sreenath, M.C., Hubert Joe, I., Rastogi, V.K., 2018. Third-order optical nonlinearities of 1,5-Diaminoanthraquinone for optical limiting application. Opt. Laser Technol. 108, 218–234. https://doi.org/10.1016/j.optlastec.2018.06.056.
Studio, A.D., n.d. 1.7, Accelrys Software Inc., San Diego, CA, USA. 2006.
Sun, H., 1998. COMPASS: an ab initio force-field optimized for condensed-phase applications overview with details on alkane and benzene compounds. J. Phys. Chem. B 102, 7338–7364.
Tapia, O., Goscinski, O., 1975. Self-consistent reaction field theory of solvent effects. Mol. Phys. 29, 1653–1661.
Villegas, L.G.C., Mashhadi, N., Chen, M., Mukherjee, D., Taylor, K.E., Biswas, N., 2016. A short review of techniques for phenol removal from wastewater. Curr. Pollut. Rep. 2, 157–167.
Vosoughi, M., Fatehifar, E., Derafshi, S., Rostamizadeh, M., 2017. High efficient treatment of the petrochemical phenolic effluent using spent catalyst: Experimental and optimization. J. Environ. Chem. Eng. 5, 2024–2031. https://doi.org/10.1016/j.jece.2017.04.003.

Wang, X.-G., Weiss, W., Shaikhutdinov, S.K., Ritter, M., Petersen, M., Wagner, F., Schlögl, R., Scheffler, M., 1998. The hematite (α-Fe2O3)(0001) surface: evidence for domains of distinct chemistry. Phys. Rev. Lett. 81, 1038.

Wang, Y., Wang, J., Deng, R., Xv, S., Lv, X., Zhou, J., Li, S., Cao, F., Qin, G., 2018. Preparation and photocatalytic property of porous α-Fe2O3 nanoflowers. Mater. Res. Bull. 107, 94–99.

Weiss, W., Ranke, W., 2002. Surface chemistry and catalysis on well-defined epitaxial iron-oxide layers. Prog. Surf. Sci. 70, 1–151.

Xavier, R.J., Gobinath, E., 2012. FT-IR, FT-Raman, ab initio and DFT studies, HOMO–LUMO and NBO analysis of 3-amino-5-mercapto-1,2,4-triazole. Spectrochim. Acta. A. Mol. Biomol. Spectrosc. 86, 242–251. https://doi.org/10.1016/j.saa.2011.10.031.

Xia, L., Ju, J., Xu, W., Ding, C., Cheng, B., 2016. Preparation and characterization of hollow Fe2O3 ultra-fine fibers by centrifugal spinning. Mater. Des. 96, 439–445. https://doi.org/10.1016/j.matdes.2016.02.053.

Yang, C., Qian, Y., Zhang, L., Feng, J., 2006. Solvent extraction process development and on-site trial-plant for phenol removal from industrial coal-gasification wastewater. Chem. Eng. J. 117, 179–185.

Yang, X., Xia, L., Li, J., Dai, M., Yang, G., Song, S., 2017. Adsorption of As(III) on porous hematite synthesized from goethite concentrate. Chemosphere 169, 188–193. https://doi.org/10.1016/j.chemosphere.2016.11.061.

Yoon, S.U., Mahanty, B., Ha, H.M., Kim, C.G., 2016. Phenol adsorption on surface-functionalized iron oxide nanoparticles: modeling of the kinetics, isotherm, and mechanism. J. Nanoparticle Res. 18, 170.

Zhang, Q., Jing, R., Zhao, S., Wu, M., Liu, X., Shao, Y., Lv, F., Liu, A., Meng, Z., 2019. Adsorption of cationic and anionic dyes on montmorillonite in single and mixed wastewater. J. Porous Mater. 26, 1861–1867. https://doi.org/10.1007/s10934-019-00782-2.

Zhu, L., Lou, B., Yang, K., Chen, B., 2005. Effects of ionizable organic compounds in different species on the sorption of p-nitroaniline to sediment. Water Res. 39, 281–288.